

STAR-RIS Aided Integrated Sensing, Computing, and Communication for Internet of Robotic Things

Haochen Li, *Graduate Student Member, IEEE*, Xidong Mu, *Member, IEEE*, Yuanwei Liu, *Fellow, IEEE*, Yue Chen, *Senior Member, IEEE*, Pan Zhiwen, *Member, IEEE*,

Abstract—A simultaneously transmitting and reflecting reconfigurable intelligent surface (STAR-RIS) aided integrated sensing, computing, and communication (ISCC) Internet of Robotic Things (IoRT) framework is proposed. Specifically, the full-duplex (FD) base station (BS) simultaneously receives the offloading signals from decision robots (DRs) and carries out target robot (TR) sensing. A computation rate maximization problem is formulated to optimize the sensing and receive beamformers at the BS and the STAR-RIS coefficients under the BS power constraint, the sensing signal-to-noise ratio constraint, and STAR-RIS coefficients constraints. The alternating optimization (AO) method is adopted to solve the proposed optimization problem. With fixed STAR-RIS coefficients, the sub-problem with respect to sensing and receiving beamformer at the BS is tackled with the weighted minimum mean-square error method. Given beamformers at the BS, the sub-problem with respect to STAR-RIS coefficients is tackled with the penalty method and successive convex approximation method. The overall algorithm is guaranteed to converge to at least a stationary point of the computation rate maximization problem. Our simulation results validate that the proposed STAR-RIS aided ISCC IoRT system can enhance the sum computation rate compared with the benchmark schemes.

Index Terms—Simultaneously transmitting and reflecting reconfigurable intelligent surface; integrated sensing, computing, and communication; Internet of Robotic Things.

I. INTRODUCTION

The Internet of Things (IoT) has catalyzed transformative advances in connectivity and automation by enabling seamless interaction between physical devices and the digital world [1, 2]. Within this landscape, the Internet of Robotic Things (IoRT) emerges as a specialized paradigm that leverages robotic systems to collect, transmit, and analyze data in diverse environments, ranging from terrestrial landscapes to air and water [3, 4]. IoRT offers unprecedented opportunities for remote sensing, exploration, and autonomous operation in

environments where direct human presence is impractical or hazardous [5, 6].

Despite its promising potential, IoRT faces multifaceted challenges that impede its widespread adoption and operational efficacy. These challenges encompass technical limitations associated with environment perception [7], onboard computation [8], and communication reliability [9]. Addressing these challenges is imperative to unlock the full capabilities of IoRT and realize its transformative impact across various domains, including disaster response, environmental monitoring, industrial automation, and infrastructure management.

In terms of environment perception, the localization of robots plays a critical role in enabling efficient and safe navigation within IoRT systems. By continuously updating and tracking the positions of robots, the BS can dynamically plan optimal paths to avoid collisions [10] and optimize robot movements based on real-time environmental conditions and task requirements [11]. This capability is particularly crucial in scenarios where multiple robots operate concurrently in shared environments [12]. Through active sensing, the position of the target robots can be obtained by the BS [13].

Onboard computation is of vital importance for automatic robots. With the ability to actively acquire information, the automatic robots can spontaneously make decisions and decide on the following actions. However, the decision-making process for automatic robots often entails computationally intensive tasks, posing challenges due to the limited power and central processing unit (CPU) resources of mobile robots, potentially becoming bottlenecks for instant on-board computing [14]. To address this limitation, the concept of mobile edge computing (MEC) has been introduced, allowing computation tasks to be offloaded to powerful MEC servers located at BSs [15]. By leveraging MEC, automatic robots can transfer computation-intensive tasks to the MEC servers, where they are processed efficiently. For mobile robots supported by onboard batteries, energy consumption limitations are critical. With mobile edge computing, robots can offload part of their computation to edge servers, thereby reducing their power consumption.

The successful implementation of MEC relies heavily on reliable communication links between robots and BSs [16]. However, challenges arise when wireless channels between the BS and robots are obstructed by static or moving obstacles, which can significantly impede the efficiency of task offloading for the robots [17]. Reconfigurable intelligent surfaces (RIS) offer a potential solution to this issue. Equipped with numerous reflecting elements, a RIS can dynamically

Copyright (c) 20xx IEEE. Personal use of this material is permitted. However, permission to use this material for any other purposes must be obtained from the IEEE by sending a request to pubs-permissions@ieee.org. (Corresponding author: Yuanwei Liu and Pan Zhiwen.)

Haochen Li and Pan Zhiwen are with National Mobile Communications Research Laboratory, Southeast University, Nanjing 210096, China, and also with Purple Mountain Laboratories, Nanjing 211100, China (email: lihaochen@seu.edu.cn, pzw@seu.edu.cn).

Xidong Mu is with the Centre for Wireless Innovation (CWI), Queen's University Belfast, Belfast, BT3 9DT, U.K. (e-mail: x.mu@qub.ac.uk).

Yuanwei Liu is with the Department of Electrical and Electronic Engineering, The University of Hong Kong, Hong Kong (e-mail: yuanwei@hku.hk).

Yue Chen is with the School of Electronic Engineering and Computer Science, Queen Mary University of London, London E1 4NS, U.K. (e-mail: yue.chen@qmul.ac.uk).

adjust the propagation of wireless signals incident upon it by tuning the phase shift of each element [18–20]. Based on the aforementioned analysis, the RIS aided integrated sensing, computing, and communication (ISCC) framework is a promising architecture for IoRT.

A. Prior Works

The paradigm for ISCC systems can be categorized into two main approaches: user-sensing based ISCC and BS-sensing based ISCC. In the user-sensing based ISCC approach, users are required to simultaneously carry out sensing and communication tasks (dual function) [21–26]. The authors in [21] focus on jointly designing sensing and offloading beamformers for IoT users with the goal of maximizing energy efficiency within the ISCC system, which is crucial for the sustainable operation of battery-powered IoT devices. Meanwhile, [22] and [23] explore the utilization of unmanned aerial vehicles (UAVs) as dual-function users in ISCC systems. In [22], the UAV trajectory is optimized to maximize the energy and time consumption. In [23], the optimization of UAV trajectories and offloading beamformers is carried out with the objective of achieving a trade-off between task offloading rate and sensing beam pattern gain. The above works are limited to single device cases and thus are not applicable to IoRT systems where multiple robots need service from the same BS. The authors of [24] and [25] investigated the ISCC system with multiple users. In [24], the authors propose a novel approach using multi-objective optimization to optimize the transmit waveforms of users in an ISCC system with dual function users aiming to emulate an ideal radar beam pattern while controlling offloading energy consumption. In [25], the authors focus on addressing the challenges of multi-cell interference environments in ISCC systems by solving a joint device association and subchannel assignment problem. To provide reliable and low-latency edge computing service for fault-sensitive applications, a ISCC system with short-packet transmissions is investigated in [26].

For the user-sensing based ISCC, the performance of the sensing and communication tasks are constrained from three aspects. Firstly, dual-function users incur higher power consumption due to the simultaneous execution of sensing and communication tasks. This increased power demand is particularly challenging in IoRT environments where robots are often powered by onboard batteries. Secondly, the deployment of antenna arrays on mobile users is constrained by size limitations, which can restrict the sensing performance of these devices. Lastly, designing and implementing advanced hardware that supports both sensing and communication functionalities can increase complexity and cost, potentially limiting the scalability and deployment flexibility of IoRT networks. Thus, it is necessary to explore the BS-sensing based ISCC systems for IoRT.

Works [27–30] investigated the BS-sensing based ISCC. In [27], the authors employ time division multiple access (TDMA) to partition the ISCC system into distinct communication, sensing, and offloading phases within different time slots. The proposed sum communication and compu-

tation rate maximization problem is tackled with an optimized time partitioning policy. In a similar time division manner, authors in [28] proposed a sensing-centric ISCC system where the object of sensing service is to achieve action recognition. A sensing accuracy maximization problem is solved under the communication and computation quality of service requirements. However, the limited time available for each function in traditional TDMA schemes may lead to inefficiencies in system design, motivating the need for more integrated approaches. To achieve simultaneous sensing, communication, and computation, authors in [29] proposed a RIS-aided ISCC system. The sum terminal energy consumption is minimized under the sensing and computation constraints. Furthermore, authors in [30] proposed an ISCC system with radio-frequency-chain-free users and adopted the RIS as a passive transmitter instead of a passive relay. This scheme is promising in IoT systems where the terminal devices are cost and energy limited.

B. Motivations and Contributions

When adopting the conventional RIS to facilitate the offloading links between the robots and the BS, the robots must be situated on the same side of the RIS. This geographical restriction may not always be satisfied in real communication systems, especially for mobile robots in IoRT systems. As a remedy, the concept of simultaneously transmitting and reflecting RISs (STAR-RISs) is used to address this limitation [31]. Although conventional reflecting-only RISs can cover all robots when they are deployed at the end of the zone, the STAR-RISs can provide larger coverage and better channels than conventional RISs [32,33]. STAR-RIS technology partitions the incoming signal into transmission and reflection regions simultaneously. This innovative approach enables full-space coverage and provides additional degrees of freedom (DoFs) for beamforming design, paving the way for more efficient and reliable communication in dynamic robotic environments.

Given these advantages, the STAR-RIS aided ISCC framework holds promise as an architecture for IoRT. However, the full space coverage and increased DoFs introduced by STAR-RIS also pose new challenges in system design. Firstly, there are additional optimization factors to consider, such as phase shifts and amplitudes for both transmission and reflection. Secondly, the STARS beamforming arrangement imposes additional coupling constraints, significantly increasing the design's complexity. These obstacles lead to new optimization problems compared with conventional RIS beamforming and encourage us to study STAR-RIS aided ISCC in IoRT systems. To our knowledge, there is no prior research on STAR-RIS for ISCC.

Contributions of this paper can be summarized as follows:

- A novel STAR-RIS aided ISCC IoRT framework is first proposed. This framework aims to establish reliable communication links for robots that require MEC services and enable sensing of specific robot of interest by the base station BS. The problem of maximizing the sum computation rate is formulated to optimize the beamformers

at the BS and the coefficients of the STAR-RIS under constraints including the BS power constraint, the sensing signal-to-interference-plus-noise ratio (SINR) constraint, and constraints on the STAR-RIS coefficients.

- We first reformulate the sensing constraint in the proposed optimization problem using an equivalent communication model. Subsequently, the reformulated problem is tackled using the alternating optimization (AO) method. The sensing/receiving beamformers at the BS and the coefficients of the STAR-RIS, are optimized iteratively with each other fixed during alternating steps. With fixed STAR-RIS coefficients, the sub-problem with respect to sensing and receiving beamformer at the BS is tackled with the weighted minimum mean-square error (WMMSE) method. Given beamformers at the BS, the rank constraint in the sub-problem with respect to STAR-RIS coefficients is tackled with the penalty based method. The resulting problem from the penalty-based approach is then solved using the successive convex approximation method. The proposed algorithm is guaranteed to converge to at least a stationary point of the computation rate maximization problem.
- The simulation results demonstrate that the proposed AO algorithm for solving the proposed sum computation rate maximization problem can converge. Besides, the sum computation rate depends on multiple parameters in the ISCC IoRT system, including the sensing threshold, the power available at the BS, and the number of RIS elements. Additionally, the advantage of adopting STAR-RIS in ISCC IoRT system is verified.

C. Organization and Notations

The remainder of this paper is organized as follows: Section II provides the system model for the proposed ISCC IoRT system, where the STAR-RIS model, signal model, communication model, sensing model, and computation model are introduced. Section III presents the problem formulation for the sum computation rate maximization problem and employs an AO-based approach to address the optimization problem. Section IV discusses simulation results, while Section V concludes this paper.

Lowercase, uppercase, and bold lowercase letters denote scalars, vectors, and matrices, respectively. The space of $M \times K$ dimensional complex matrices is denoted as $\mathbb{C}^{M \times K}$. The superscripts $(\cdot)^T$, $(\cdot)^*$, and $(\cdot)^H$ signify transpose, conjugate, and conjugate transpose operations, respectively. The vector containing the main diagonal elements of matrix \mathbf{A} is expressed as $\text{diag}(\mathbf{A})$. $\text{Bdiag}(\cdot)$ denotes the block diagonal operations. The functions $\text{tr}(\mathbf{A})$ and $\text{rank}(\mathbf{A})$ refer to the trace and rank of matrix \mathbf{A} . The real component of a complex number is extracted using $\Re(\cdot)$. The absolute value of a complex number is represented by $|\cdot|$. Sets are denoted using calligraphic letters, such as \mathcal{A} .

II. SYSTEM MODEL

As shown in Fig. 1, a STAR-RIS aided ISCC system for IoRT is proposed, where the full-duplex (FD) BS equipped

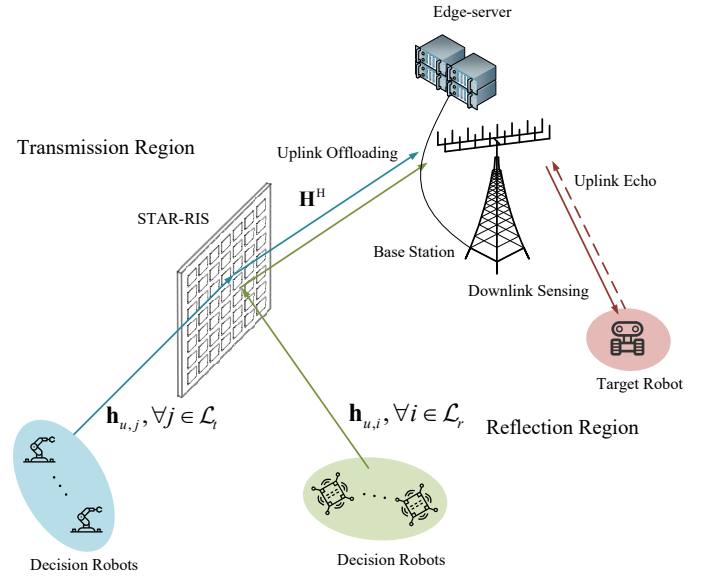


Fig. 1: The system model for the proposed STAR-RIS aided integrated sensing, computing, and communication system.

with an edge server simultaneously provides edge computing services for L decision robots (DRs) and senses a target robot (TR) in its vicinity. The DR refers to the robot equipped with various sensors such as temperature sensors, humidity sensors, magnetic field sensors, etc., and has the ability to autonomously make decisions. The TR refers to the robot that the BS intends to sense. The block fading channel model is adopted, where the channel characteristics remain constant within each coherence block and vary between different coherence blocks. The robots are assumed to be stationary within each channel coherence time. The FD BS is equipped with N_t transmit antennas and N_r receive antennas. All DRs are equipped with single antenna. The direct links between the BS and DRs are blocked with obstacles and an N -element STAR-RIS is deployed to establish extra communication links between them. The indices for DRs and RIS elements are collected in sets $\mathcal{L} = \{1, 2, \dots, L\}$ and $\mathcal{N} = \{1, 2, \dots, N\}$, respectively. The indices for DRs in the reflection region and the transmission region of the STAR-RIS are collected in sets \mathcal{L}_r and \mathcal{L}_t , respectively. The FD BS sends the downlink sensing through the transmit uniform linear array (ULA) and collects the uplink offloading signals from DRs as well as the echo signal from the TR using a receive ULA. The structure of the considered FD BS is given in Fig. 2.

A. STAR-RIS Model

Unlike conventional RIS with non-magnetic elements in STAR-RIS can re-radiate the signals impinging on it in both reflection manner and transmission manner. For the n -th element in the RIS, define reflection coefficient $\phi_n^t = \sqrt{\rho_n^t} e^{j\theta_n^t}$ and transmission coefficient $\phi_n^r = \sqrt{\rho_n^r} e^{j\theta_n^r}$ to characterize its reflection and transmission performance. Specifically, ρ_n^t and ρ_n^r are the amplitude coefficients of the n -th STAR element, while $\theta_n^t \in [0, 2\pi)$ and $\theta_n^r \in [0, 2\pi)$ are the phase coefficients of the n -th STAR element. With coefficients defined above, the transmission and reflection matrices of the STAR-RIS can be given

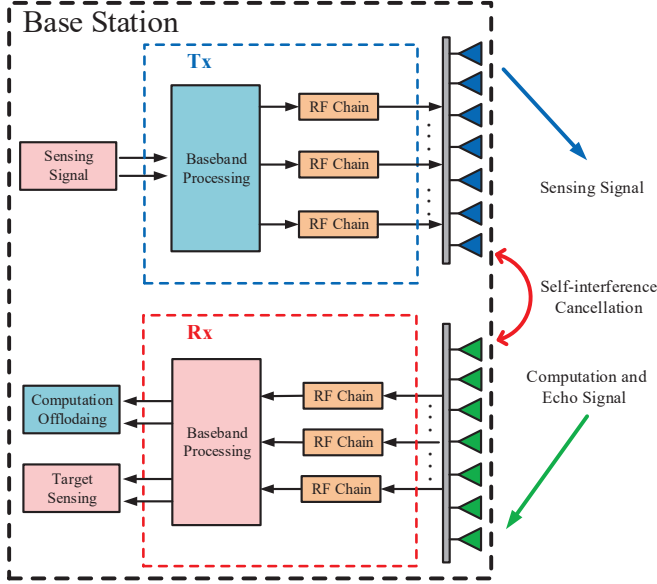


Fig. 2: The structure of the full duplex integrated sensing, computing, and communication base station.

as $\Phi_i = \text{diag}(\sqrt{\rho_1^i} e^{j\theta_1^i}, \sqrt{\rho_2^i} e^{j\theta_2^i}, \dots, \sqrt{\rho_N^i} e^{j\theta_N^i})$, $\forall i \in \{t, r\}$. Since the STAR-RIS is a passive equipment, the amplitude coefficients of each element should satisfy the law of conservation of energy, which can be expressed as

$$\rho_n^t + \rho_n^r = 1, \rho_n^i \geq 0, \forall i \in \{t, r\}. \quad (1)$$

B. Signal Model

The signal transmitted from the BS is given as

$$\mathbf{x} = \mathbf{w}d, \quad (2)$$

where $\mathbf{w} \in \mathbb{C}^{N_t \times 1}$ represents the sensing beamformer. d is the sensing signal with normalized power. The power consumption for sensing at the BS can be given as $P_d = \mathbb{E}\{\mathbf{x}^H \mathbf{x}\} = \mathbf{w}^H \mathbf{w}$.

The signal received at the BS contains the uplink offloading signals from the DRs, the echo sensing signal, and the self-interference signal. It can be expressed as

$$\tilde{\mathbf{y}} = \underbrace{\sum_{l=1}^L \sqrt{P_u} \mathbf{H}^H \Phi(l) \mathbf{h}_{u,l} c_l}_{\text{uplink offloading signal}} + \underbrace{\mathbf{A} \mathbf{x}}_{\text{echo sensing signal}} + \underbrace{\mathbf{H}_{SI} \mathbf{x}}_{\text{self-interference}} + \mathbf{n}, \quad (3)$$

where $\mathbf{H} \in \mathbb{C}^{N \times N_r}$ is the channel from the BS to the RIS. $\mathbf{h}_{u,l} \in \mathbb{C}^{N \times 1}$, $\forall l \in \mathcal{L}$, is the channel from the DR l to the RIS. $c_l \in \mathbb{C}$, $\forall l \in \mathcal{L}$, is the information symbol from DR l with normalized power. P_u is the transmit power of DRs. \mathbf{A} and \mathbf{H}_{SI} are the sensing channel and the self-interference channel between two ULAs at the BS, respectively. $\mathbf{n} \sim \mathcal{CN}(\mathbf{0}, \sigma_u^2 \mathbf{I})$ is the AWGN at the receiver of the BS and σ_u^2 is the noise power. $\Phi(l) = \Phi_r$ when $l \in \mathcal{L}_r$; $\Phi(l) = \Phi_t$ when $l \in \mathcal{L}_t$.

The difficulty for FD BS design lies in that the transmit and receive antenna arrays are co-located at the FD BS. The outgoing signal from the BS may overwhelm its receive

hardware with limited-dynamic-range, making it challenging to extract useful signals at the BS [34]. Solutions like hardware isolation, analog and digital cancellation are proposed to carry out self-interference cancellation [35, 36], which can achieve 100 dB SI suppression [37]. Thus, the self-interference after suppression is omitted in this work. The signal received at the BS after self-interference cancellation is given by

$$\mathbf{y} = \sum_{l=1}^L \sqrt{P_u} \mathbf{H}^H \Phi(l) \mathbf{h}_{u,l} c_l + \mathbf{A} \mathbf{x} + \mathbf{n}. \quad (4)$$

Note that the TR is assumed to be located in the vicinity of the BS and the channels between the BS and the TR can be modeled with line-of-sight (LoS) channels. The antenna spacing of the ULAs adopted at the BS is half wavelength. When detecting the TR at an angle of interesting θ_0 , the array response vector between the BS transmitting antenna and the TR is [38]

$$\mathbf{a}_t(\theta_0) = \frac{1}{\sqrt{N_t}} [1, e^{j \sin(\theta_0)}, \dots, e^{j(N_t-1) \sin(\theta_0)}]^T. \quad (5)$$

The array response vector between the BS receiving antenna and the TR is

$$\mathbf{a}_r(\theta_0) = \frac{1}{\sqrt{N_r}} [1, e^{j \sin(\theta_0)}, \dots, e^{j(N_r-1) \sin(\theta_0)}]^T. \quad (6)$$

The sensing channel between the BS and the target can be expressed as

$$\mathbf{A}_0 = \alpha_0 \mathbf{a}_r(\theta_0) \mathbf{a}_t(\theta_0)^H, \quad (7)$$

where α_0 is the complex sensing coefficient decided by the radar cross-section of the TR and the path loss between the BS and the TR. Assume there are M interferences distributed across M different angles, i.e., $\theta_1, \theta_2, \dots, \theta_M$ [39]. The sensing channel between the BS and interferences can be expressed as

$$\mathbf{A}_I = \sum_m \mathbf{A}_m = \sum_m \alpha_m \mathbf{a}_r(\theta_m) \mathbf{a}_t(\theta_m)^H, \quad (8)$$

where α_m is the complex sensing coefficient decided by the radar cross-section of the m -th interfere and the path loss between the BS and the m -th interfere.

The sensing channel can be expressed as

$$\mathbf{A} = \mathbf{A}_0 + \mathbf{A}_I = \sum_{m=0}^M \mathbf{A}_m. \quad (9)$$

In this work, the RIS is deployed near the DRs which are blocked by obstacles to establish communication links for them. The TR is in the vicinity of the BS. Therefore, the RIS-related sensing link may not exist due to an unfavorable wireless path between the RIS and the TR. Besides, even if the RIS-related sensing link exists, the sensing signals need to experience the BS-RIS-target-BS path to reach the BS. The long propagation distance and the double fading introduced by the RIS lead to limited echo signal power. As a result, the sensing signal reflected by the RIS is omitted at the receiver of the BS in this work.

C. Communication Model and Sensing Model

In this section, the communication model for the uplink computation offloading for DRs and the sensing model for probing the TR are introduced. Assign receive beamformer \mathbf{u}_l for extracting information for DR l from received signal \mathbf{y} at the BS. The uplink communication SINR for DR l can be expressed as in (11) at the top of the next page, wherein

$$\mathbf{R}_l = P_u \sum_{i \neq l} \mathbf{H}^H \Phi(i) \mathbf{h}_{u,i}^H \mathbf{h}_{u,i}^H \mathbf{H} \Phi(i) + \mathbf{A} \mathbf{w} \mathbf{w}^H \mathbf{A}^H + \sigma_u^2 \mathbf{I}_{N_r}. \quad (10)$$

The achievable communication rate for DR l can be given as

$$R_{u,l} = \log(1 + \gamma_{u,l}), \forall l \in \mathcal{L}. \quad (12)$$

In this work, we adopt conventional BS sensing for the sensing function. Upon extracting the uplink offloading signals from DRs, the BS carries out successive interference cancellations to remove the decoded offloading signals from the received signal [40]. Assuming perfect successive interference cancellation at the BS, the signal for target sensing can be given as

$$\mathbf{y}_s = \mathbf{A} \mathbf{x} + \mathbf{n}. \quad (13)$$

In sensing systems, the sensing accuracy of the target is often a monotonically increasing function of the sensing SINR [41]. Thus, we adopt the sensing SINR as the performance measure for the sensing feature, which can be expressed as

$$\gamma_{rad} = \frac{\mathbf{u}^H \mathbf{A}_0 \mathbf{w} \mathbf{w}^H \mathbf{A}_0^H \mathbf{u}}{\mathbf{u}^H \mathbf{A}_I \mathbf{w} \mathbf{w}^H \mathbf{A}_I^H \mathbf{u} + \sigma_u^2 \|\mathbf{u}\|_2^2}, \quad (14)$$

where \mathbf{u} represents the receive beamformer for target sensing. The sensing performance of the system can be ensured by setting a relatively large sensing SINR requirement.

D. Computation Model

In this section, we introduce the computation model for the proposed ISCC system for the IoRT. Due to limited computation ability and power, the DRs offload their computation tasks to the edge server at the BS through uplink transmission links. Compared to binary offloading, partial offloading has the benefit of making greater use of parallel computing resources and available bandwidth. It enables flexible component/data splitting, and by assigning time- or energy-consuming sub-tasks to MEC servers, it can result in increased energy savings and decreased computation delays [15]. The delay caused by the computing at the edge server and the return of the computation results to the DRs is omitted considering the superior computing power of the edge server and the limited size of the computation results.

The edge server allocates CPU-cycle frequency (cycle/s) f_l for the DR l to execute a computation task that requires ϕ computation cycles to process one bit of data. Under this configuration, the computation rate of DR l at the BS can be given by

$$r_l = \frac{f_l}{\phi}, \forall l \in \mathcal{L}. \quad (15)$$

The power required to execute the computation task for DR l can be given as

$$P_l = \kappa f_l^3 = \kappa (\phi r_l)^3, \forall l \in \mathcal{L}, \quad (16)$$

where κ is the power coefficient decided by the CPU chip architecture at the edge server. Note that the communication capacity between the DRs and the BS is limited, the computation rate of DRs should satisfy the following constraints

$$r_l \leq B R_{u,l}, \forall l \in \mathcal{L}, \quad (17)$$

where B is the communication bandwidth for uplink offloading. Constraint (17) arises from the communication-computation causality principle, whereby the maximum number of bits processed by the edge server for DR l must not surpass the transmission capacity of the link connecting the BS and DR l . The sum computation rate of DRs is

$$R = \sum_{l=1}^L r_l. \quad (18)$$

III. FD ISCC DESIGN FOR COMPUTATION RATE MAXIMIZATION

A. Optimization Problem Formulation

In this work, we aim to maximize the sum computation rate of DRs by optimizing the sensing beamformer \mathbf{w} , receive beamformers $\mathbf{u}_l, \forall l$, and the STAR-RIS reflection matrices Φ_r, Φ_t . The sum computation maximization problem can be given as

$$\max_{\mathcal{A}} R \quad (19a)$$

$$\text{s.t. } \gamma_{rad} \geq \Gamma_{rad}, \quad (19b)$$

$$r_l \leq B R_{u,l}, \forall l \in \mathcal{L}, \quad (19c)$$

$$P_d + \sum_{l=1}^L P_l \leq P_b, \quad (19d)$$

$$\theta_n^i \in (0, 2\pi], \forall n \in \mathcal{N}, i \in \{t, r\}, \quad (19e)$$

$$\rho_n^i \in [0, 1], \forall n \in \mathcal{N}, i \in \{t, r\}, \quad (19f)$$

$$\rho_n^t + \rho_n^r = 1, \forall n \in \mathcal{N}, \quad (19g)$$

where $\mathcal{A} = \{\mathbf{w}, \mathbf{u}, \{\mathbf{u}_l\}_{l=1}^L, \{r_l\}_{l=1}^L, \Phi_r, \Phi_t\}$ is the set for optimization variables. P_b is the power budget of the BS. P_d and P_l are the power consumption for sensing and the power consumption for executing the computation task for DR l , respectively. Constraint (19b) ensures that the minimum SINR for radar operations exceeds the designated sensing threshold Γ_{rad} . Constraint (19c) ensures that the computation bits processed by the edge server for DR l are less than the communication capacity of the offloading link. Constraint (19d) limits the power consumption for sensing and computation under the power budget of the BS. Constraints (19e)-(19g) are the STAR-RIS coefficients constraint.

Remark 1. offloading-sensing trade-off: Both target sensing and offloading computation consume the limited power budget at the BS, giving rise to an inherent offloading-sensing trade-off. As more data is offloaded to the BS's edge server, the edge server consumes more power. Consequently, less power

$$\begin{aligned}
\gamma_{u,l} &= \frac{P_u \mathbb{E}\{|\mathbf{u}_l^H \mathbf{H}^H \Phi(l) \mathbf{h}_{u,l} c_l|^2\}}{P_u \sum_{i \neq l} \mathbb{E}\{|\mathbf{u}_l^H \mathbf{H}^H \Phi(i) \mathbf{h}_{u,i} c_i|^2\} + \mathbb{E}\{|\mathbf{u}_l^H \mathbf{A} \mathbf{x}|^2\} + \mathbb{E}\{|\mathbf{u}_l^H \mathbf{n}|^2\}} \\
&= \frac{P_u |\mathbf{u}_l^H \mathbf{H}^H \Phi(l) \mathbf{h}_{u,l}|^2}{P_u \sum_{i \neq l} |\mathbf{u}_l^H \mathbf{H}^H \Phi(i) \mathbf{h}_{u,i}|^2 + \mathbf{u}_l^H \mathbf{A} \mathbf{w} \mathbf{w}^H \mathbf{A}^H \mathbf{u}_l + \sigma_u^2 \|\mathbf{u}_l\|_2^2} \\
&= \frac{P_u \mathbf{u}_l^H \mathbf{H}^H \Phi(l) \mathbf{h}_{u,l} \mathbf{h}_{u,l}^H \Phi(l)^H \mathbf{H} \mathbf{u}_l}{\mathbf{u}_l^H \mathbf{R}_l^H \mathbf{u}_l}.
\end{aligned} \tag{11}$$

is available for target sensing, which can lead to unsatisfying sensing performance. Conversely, allocating more power to target sensing reduces the power available for computing the offloaded data at the BS, which may result in degraded offloading performance.

B. Equivalent Communication Model for the Sensing Constraint

An equivalent multiple-input and multiple-output (MIMO) communication system is proposed, wherein the SINR of the MIMO system has the same form as the sensing SINR of the ISCC system. Then, we replace the sensing SINR constraint (19b) with the equivalent MIMO communication capacity constraint. Assuming there is a N_t -antenna BS communicates with a N_r -antenna user, the signal received by the user can be given as

$$\mathbf{y}_{rad} = \mathbf{A}_0 \mathbf{w} d + \mathbf{n}_{rad}, \tag{20}$$

where d is the transmitted signal of the equivalent communication system and \mathbf{w} is the beamformer for the transmitted signal. \mathbf{A}_0 is the channel between the BS and the user. \mathbf{n}_{rad} is the noise vector with covariance matrix $\mathbf{R}_{rad} = \mathbf{A}_I \mathbf{w} \mathbf{w}^H \mathbf{A}_I + \sigma_u^2 \mathbf{I}_{N_r}$. The capacity of the equivalent communication system can be expressed as [42]

$$\begin{aligned}
R_{rad} &= \log \left(1 + \frac{\mathbf{u}^H \mathbf{A}_0 \mathbf{w} \mathbf{w}^H \mathbf{A}_0^H \mathbf{u}}{\mathbf{u}^H \mathbf{A}_I \mathbf{w} \mathbf{w}^H \mathbf{A}_I^H \mathbf{u} + \sigma_u^2 \|\mathbf{u}\|_2^2} \right) \\
&= \log(1 + \gamma_{rad}).
\end{aligned} \tag{21}$$

Define $r_{rad} = \log(1 + \Gamma_{rad})$. The constraint (19b) can be reformulated as

$$r_{rad} \leq R_{rad}. \tag{22}$$

The sum computation maximization problem can be given as

$$\max_{\mathcal{A}} R \tag{23a}$$

$$\text{s.t. } r_{rad} \leq R_{rad}, \tag{23b}$$

$$(19c) - (19g), \tag{23c}$$

where constraints (19c)-(19g) are the DR offloading constraint, the power constraint of the BS, and the STAR-RIS coefficients constraint.

The AO method is adopted to tackle problem (23), where the variables $\mathcal{B} = \{\mathbf{w}, \mathbf{u}, \{\mathbf{u}_l\}_{l=1}^L, \{r_l\}_{l=1}^L\}$ is optimized with fixed variables $\mathcal{C} = \{\Phi_r, \Phi_t\}$, and vice versa.

C. Optimization Problem with respect to \mathcal{B}

With fixed STAR-RIS matrix coefficients Φ_r and Φ_t , the sum computation rate maximization problem can be expressed

as

$$\max_{\mathcal{B}} \sum_{l=1}^L r_l \tag{24a}$$

$$\text{s.t. } (23b), (19c), \tag{24b}$$

$$\mathbf{w}^H \mathbf{w} + \sum_{l=1}^L \kappa(\phi r_l)^3 \leq P_b. \tag{24c}$$

Problem (24) is non-convex since constraints (23b) and (19c) are non-convex. To tackle the non-convex constraint (19c), the WMMSE method is adopted [43]. With \mathbf{u} and \mathbf{u}_l decoding the signal of the equivalent communication system and the offloading signals from the DR l , respectively, the decoded signals for the equivalent communication system and the DR l can be expressed as

$$\hat{d} = \mathbf{u}^H \mathbf{y}_{rad}, \tag{25}$$

$$\hat{c}_l = \mathbf{u}_l^H \mathbf{y}, \tag{26}$$

The mean square error (MSE) of the signal of the equivalent communication system and the signal transmitted from DR l are

$$e_{rad} = \mathbb{E}[|\hat{d} - d|^2] = \mathbf{u}^H \mathbf{R}_1 \mathbf{u} - 2\Re(\mathbf{u}^H \mathbf{A}_0 \mathbf{w}) + 1, \tag{27}$$

$$e_l = \mathbb{E}[|\hat{c}_l - c_l|^2] = \mathbf{u}_l^H \mathbf{R}_2 \mathbf{u}_l - 2\sqrt{P_u} \Re(\mathbf{u}_l^H \mathbf{H}^H \Phi(l) \mathbf{h}_{u,l}) + 1, \tag{28}$$

where \mathbf{R}_1 is the covariance matrix of the signal received at the equivalent communication system, which can be expressed as

$$\begin{aligned}
\mathbf{R}_1 &= \mathbb{E}[\mathbf{y}_{rad} \mathbf{y}_{rad}^H] \\
&= \mathbf{A}_0 \mathbf{w} \mathbf{w}^H \mathbf{A}_0^H + \mathbf{A}_I \mathbf{w} \mathbf{w}^H \mathbf{A}_I^H + \sigma_u^2 \mathbf{I}_{N_r}.
\end{aligned} \tag{29}$$

\mathbf{R}_2 is the covariance matrix of the signal received at the BS of the ISCC system, which can be expressed as

$$\begin{aligned}
\mathbf{R}_2 &= \mathbb{E}[\mathbf{y} \mathbf{y}^H] \\
&= \sum_l \mathbf{H}^H \Phi(l) \mathbf{h}_{u,l} \mathbf{h}_{u,l}^H \Phi(l)^H \mathbf{H} + \mathbf{A} \mathbf{w} \mathbf{w}^H \mathbf{A}^H + \sigma_u^2 \mathbf{I}_{N_r}.
\end{aligned} \tag{30}$$

In the following proposition, the tight lower bounds of the capacities of the equivalent communication system as well as the uplink offloading are formulated using the rate-MMSE relationship. and the capacity of the uplink offloading of DR l , respectively.

Proposition 1. Define $\eta = \log(\lambda) - \lambda e_{rad} + 1$ with auxiliary variable $\lambda \in \mathbb{R}^+$. η servers as a tight lower bound for the

capacity of the equivalent communication system. η satisfies:

$$\max_{\lambda, \mathbf{u}} \eta = R_{rad}, \quad (31)$$

Proof. Maximizing η with respect to \mathbf{u} is equivalent to minimizing e_{rad} , i.e., the MSE of the equivalent communication system. The MMSE receive beamformer \mathbf{u} can be obtained by setting $\partial e_{rad}/\partial \mathbf{u} = 0$, which lead to

$$\mathbf{u}^* = \mathbf{R}_1^{-1} \mathbf{A}_0 \mathbf{w} \quad (32)$$

Substituting (32) into (27), the MMSE of the equivalent communication system can be expressed as

$$\begin{aligned} e_{rad}^{\text{MMSE}} &= 1 - \mathbf{w}^H \mathbf{A}_0^H \mathbf{R}_1^{-1} \mathbf{A}_0 \mathbf{w} \\ &= (1 + \mathbf{w}^H \mathbf{A}_0^H \mathbf{R}_{rad}^{-1} \mathbf{A}_0 \mathbf{w})^{-1}. \end{aligned} \quad (33)$$

Substituting (32) into (21), the capacity of the equivalent communication system can be expressed as

$$R_{rad} = \log(1 + \mathbf{w}^H \mathbf{A}_0^H \mathbf{R}_{rad}^{-1} \mathbf{A}_0 \mathbf{w}). \quad (34)$$

With given MMSE receive beamformer \mathbf{u}^{MMSE} , the λ maximizing η can be obtained by setting $\partial \eta / \partial \lambda = 0$, which lead to

$$\lambda^* = (e_{rad}^{\text{MMSE}})^{-1} \quad (35)$$

and

$$\max_{\lambda, \mathbf{u}} \eta = \log((e_{rad}^{\text{MMSE}})^{-1}). \quad (36)$$

Substituting (33) into (36), the equation (31) is established. \square

Proposition 2. Define $\eta_l = \log(\lambda_l) - \lambda_l e_l + 1$ with auxiliary variable $\lambda_l \in \mathbb{R}^+$, $\forall l \in \mathcal{L}$. η_l serves as a tight lower bound for the capacity of the uplink offloading of DR l . η_l satisfies:

$$\max_{\lambda_l, \mathbf{u}_l} \eta_l = R_{u,l}, \forall l, \quad (37)$$

Proof. The proof of proposition 2 is similar to the proof of proposition 1 and is omitted. Besides, the expression of the optimal receive beamformer and auxiliary variable for DR l is given as follows

$$\mathbf{u}_l^* = \mathbf{R}_2^{-1} \mathbf{H}^H \Phi(l) \mathbf{h}_{u,l}, \forall l, \quad (38)$$

$$\begin{aligned} e_{rad}^{\text{MMSE}} &= 1 - \mathbf{h}_{u,l}^H \Phi(l) \mathbf{H} \mathbf{R}_2^{-1} \mathbf{H}^H \Phi(l) \mathbf{h}_{u,l} \\ &= (1 + \mathbf{h}_{u,l}^H \Phi(l) \mathbf{H} \mathbf{R}_l^{-1} \mathbf{H}^H \Phi(l) \mathbf{h}_{u,l})^{-1}, \forall l, \end{aligned} \quad (39)$$

$$\lambda_l^* = (e_l^{\text{MMSE}})^{-1}, \forall l, \quad (40)$$

\square

With (31) and (37), problem (24) can be reformulated as

$$\max_{\hat{\mathcal{B}}} \sum_{l=1}^L r_l \quad (41a)$$

$$\text{s.t. } r_{rad} \leq \eta, \quad (41b)$$

$$r_l \leq \eta_l, \forall l, \quad (41c)$$

$$(24c), \quad (41d)$$

where $\hat{\mathcal{B}} = \{\mathbf{w}, \mathbf{u}, \lambda, \{\mathbf{u}_l\}_{l=1}^L, \{\lambda_l\}_{l=1}^L, \{r_l\}_{l=1}^L\}$. When the receive beamformers and auxiliary variables given by (32), (35), (38), and (40), problem (41) is convex

Algorithm 1 The Proposed Algorithm for Solving Problem (41).

- 1: Set initial sensing beamformer $\mathbf{w}^{(0)}$, $i = 0$.
- 2: Calculate $\mathbf{u}^{(i+1)}$ and $\mathbf{u}_l^{(i+1)}$, $\forall l$, based on (32) and (38).
- 3: Calculate $\lambda^{(i+1)}$ and $\lambda_l^{(i+1)}$, $\forall l$, based on (35) and (40).
- 4: Solve problem (41) with obtained receive beamformers and auxiliary variables.
- 5: Update $\{\mathbf{w}^{(i+1)}, \{r_l^{(i+1)}\}_{l=1}^L\}$.
- 6: If the fractional increase of the objective function is less than the convergence threshold, terminate. Otherwise, set $i = i + 1$ and go to step 2.

with respect to $\{\mathbf{w}, \{r_l\}_{l=1}^L\}$, which can be solved with CVX [44]. The proposed algorithm for solving problem (41) is summarized in **Algorithm 1**. The computational complexity of calculating MMSE beamformers and auxiliary variables is $\mathcal{O}(2(L+1)N_r^3)$ [45]. The computational complexity of solving convex quadratically constrained problem in step 4 is $\mathcal{O}((L+1)^{0.5}((L+1)N_t^2 + N_t^3))$ [46]. The computational complexity of **Algorithm 1** is given by $\mathcal{O}(I_1(2(L+1)N_r^3 + (L+1)^{0.5}((L+1)N_t^2 + N_t^3)))$, where I_1 is the iteration number for **Algorithm 1** to converge. The convergence of **Algorithm 1** is guaranteed by the following proposition.

Proposition 3. Algorithm 1 is guaranteed to converge to a stationary point of problem (41).

Proof. The sum computation rate of the ISCC system is bounded above due to the limited power budget at the BS. During the i -th iteration of the **Algorithm 1**, the sum computation rate satisfies (42) at the top of the next page. It can be observed that the sum computation rate is non-decreasing over every iteration. As a result, the proposed algorithm can reach at least a stationary point of problem (41). \square

D. Optimization Problem with respect to \mathcal{C}

With given variables $\mathcal{B} = \{\mathbf{w}, \mathbf{u}, \{\mathbf{u}_l\}_{l=1}^L, \{r_l\}_{l=1}^L\}$, the sum computation rate maximization problem can be expressed as

$$\text{Find } \mathcal{C} \quad (43a)$$

$$\text{s.t. } \gamma_{u,l} \geq \Gamma_{u,l}, \forall l, \quad (43b)$$

$$(19e) - (19g), \quad (43c)$$

where $\Gamma_{u,l} = e^{\frac{r_l}{B}} - 1$. Define

$$\begin{aligned} \mathbf{v}(l) &= \text{diag}(\Phi(l)), \\ &= \left[\sqrt{\rho_1^i} e^{j\theta_1^i}, \sqrt{\rho_2^i} e^{j\theta_2^i}, \dots, \sqrt{\rho_N^i} e^{j\theta_N^i} \right]^T, \forall i \in \{t, r\}, \end{aligned} \quad (44)$$

which leads to $\mathbf{v}(l) = \text{diag}(\Phi_r)$ when $l \in \mathcal{L}_r$; $\Phi(l) = \text{diag}(\Phi_t)$ when $l \in \mathcal{L}_t$. Constraint (43b) can be reformulated as

$$\begin{aligned} \frac{P_u}{\Gamma_{u,l}} \mathbf{u}_l^H \mathbf{H}^H \text{diag}(\mathbf{h}_{u,l}) \mathbf{v}(l) \mathbf{v}(l)^H \text{diag}(\mathbf{h}_{u,l}^H) \mathbf{H} \mathbf{u}_l &\geq \\ \sum_{i \neq l} P_u \mathbf{u}_i^H \mathbf{H}^H \text{diag}(\mathbf{h}_{u,i}) \mathbf{v}(i) \mathbf{v}(i)^H \text{diag}(\mathbf{h}_{u,i}^H) \mathbf{H} \mathbf{u}_i &+ N_l, \forall l, \end{aligned} \quad (45)$$

$$\begin{aligned}
& R\left(\mathbf{w}^{(i)}, \{r_l^{(i)}\}_{l=1}^L, \mathbf{u}^{(i)}, \lambda^{(i)}, \{\mathbf{u}_l^{(i)}\}_{l=1}^L, \{\lambda_l^{(i)}\}_{l=1}^L\right) \\
&= R\left(\mathbf{w}^{(i)}, \{r_l^{(i)}\}_{l=1}^L, \mathbf{u}^{(i+1)}, \lambda^{(i+1)}, \{\mathbf{u}_l^{(i+1)}\}_{l=1}^L, \{\lambda_l^{(i+1)}\}_{l=1}^L\right) \\
&\leq R\left(\mathbf{w}^{(i+1)}, \{r_l^{(i+1)}\}_{l=1}^L, \mathbf{u}^{(i+1)}, \lambda^{(i+1)}, \{\mathbf{u}_l^{(i+1)}\}_{l=1}^L, \{\lambda_l^{(i+1)}\}_{l=1}^L\right),
\end{aligned} \tag{42}$$

Algorithm 2 The Proposed Algorithm for Solving Problem (49).

- 1: Set initial STAR-RIS coefficients $\mathbf{V}_r^{(0)}$ and $\mathbf{V}_t^{(0)}$, $n = 0$.
- 2: Solve problem (51) with feasible $\mathbf{V}_r^{(n)}$ and $\mathbf{V}_t^{(n)}$.
- 3: Update $\mathbf{V}_r^{(n+1)}$ and $\mathbf{V}_t^{(n+1)}$.
- 4: If the fractional decrease of the objective function is less than the convergence threshold, terminate. Otherwise, set $n = n + 1$ and go to step 2.

where $N_l = \mathbf{u}_l^H \mathbf{A} \mathbf{w} \mathbf{w}^H \mathbf{A}^H \mathbf{u}_l + \sigma_u^2 \|\mathbf{u}_l\|_2^2$. Define $\mathbf{V}(l) = \mathbf{v}(l) \mathbf{v}(l)^H, \forall l$. Constraint (43b) can be further reformulated as

$$\frac{1}{\Gamma_{u,l}} \text{Tr}(\mathbf{B}_l^i \mathbf{V}(l)) \geq \sum_{i \neq l} \text{Tr}(\mathbf{B}_l^i \mathbf{V}(i)) + N_l, \forall l, \tag{46}$$

where $\mathbf{B}_l^i = P_u \text{diag}(\mathbf{h}_{u,i}^H) \mathbf{H} \mathbf{u}_l \mathbf{u}_l^H \mathbf{H}^H \text{diag}(\mathbf{h}_{u,i}), \forall l, i \in \mathcal{L}$.

$$\text{Find } \mathbf{V}_i, \forall i \in \{t, r\} \tag{47a}$$

$$\text{s.t. (46),} \tag{47b}$$

$$\text{rank}(\mathbf{V}_i) = 1, \forall i \in \{t, r\}, \tag{47c}$$

$$\mathbf{V}_i \succeq 0, \forall i \in \{t, r\}, \tag{47d}$$

$$\text{diag}(\mathbf{V}_t + \mathbf{V}_r) = \mathbf{I}_N. \tag{47e}$$

The problem (47) is non-convex due to the non-convex constraint (47c), which is equivalent to the following format

$$\|\mathbf{V}_i\|_* - \|\mathbf{V}_i\|_2 = 0, \forall i, \tag{48}$$

where $\|\mathbf{V}_i\|_* = \sum_j \sigma_j(\mathbf{V}_i)$ with $\sigma_j(\mathbf{V}_i)$ representing the j -th singular value (in descending order) of \mathbf{V}_i . $\|\mathbf{V}_i\|_2 = \sigma_1(\mathbf{V}_i)$ is the spectral norm of \mathbf{V}_i . For any semi-definite Hermitian matrix \mathbf{V}_i , constraint (48) is satisfied only when the constraint (47c) is met. The penalty method is used to tackle the constraint (48) [47, 48]. Introducing penalty coefficients $\rho_i, \forall i \in \{t, r\}$, the problem (47) can be reformulated as

$$\min_{\mathbf{V}_r, \mathbf{V}_t} \sum_{i \in \{t, r\}} \rho_i (\|\mathbf{V}_i\|_* - \|\mathbf{V}_i\|_2) \tag{49a}$$

$$\text{s.t. (46), (47d), (47e).} \tag{49b}$$

According to [49, Theorem 1], when ρ_i is sufficiently large, the solution to problem (49) is also feasible to problem (47). Thus, in the following, the problem (49) with large penalty coefficients are solved instead of problem (47). Problem (49) is still non-convex due to its non-convex object function. By adopting successive convex approximation (SCA) with any feasible $\mathbf{V}_r^{(n)}, \mathbf{V}_t^{(n)}$, the non-convex terms in the object function of problem (49) can be approximated as

$$\begin{aligned}
-\|\mathbf{V}_i\|_2 &\leq -\|\mathbf{V}_i^{(n)}\|_2 - \text{Tr}\left(\mathbf{b}_i^{(n)} (\mathbf{b}_i^{(n)})^H (\mathbf{V}_i - \mathbf{V}_i^{(n)})\right) \\
&= V_i^{(n)},
\end{aligned} \tag{50}$$

Algorithm 3 The Proposed Algorithm for Solving Problem (23).

- 1: Set initial $\mathbf{w}^{(0)}, \mathbf{V}_r^{(0)}$ and $\mathbf{V}_t^{(0)}$, $j = 0$.
- 2: Solve problem (41) with fixed $\mathcal{C}^{(j)}$, initial sensing beamformer with $\mathbf{w}^{(j)}$.
- 3: Update $\mathcal{B}^{(j+1)}$.
- 4: Solve problem (47) with fixed $\mathcal{B}^{(j+1)}$, initial STAR-RIS coefficients with $\mathbf{V}_r^{(j)}$ and $\mathbf{V}_t^{(j)}$.
- 5: Update $\mathcal{C}^{(j+1)}$.
- 6: If the fractional increase of the objective function is less than the convergence threshold, terminate. Otherwise, set $j = j + 1$ and go to step 2.

where $\mathbf{b}_i^{(n)}$ is the eigenvector of $\mathbf{V}_i^{(n)}$ corresponding to the singular value $\sigma_1(\mathbf{V}_i^{(n)})$. Substituting $V_i^{(n)}, \forall i$, in to the objective function, in the n -th iteration of SCA, the surrogate problem of problem (49) can be expressed as

$$\min_{\mathbf{V}_r, \mathbf{V}_t} \sum_{i \in \{t, r\}} \rho_i (\|\mathbf{V}_i\|_* + V_i^{(n)}) \tag{51a}$$

$$\text{s.t. (46), (47d), (47e).} \tag{51b}$$

Problem (51) is convex with respect to \mathbf{V}_r and \mathbf{V}_t and can be solved with CVX. The proposed algorithm for solving problem (49) is summarized in **Algorithm 2**. The computational complexity of **Algorithm 2** mainly comes from solving semidefinite programming (SDP) in step 2, which has the computational complexity of $\mathcal{O}\left(I_2 \max\{L+2, N\}^4 N^{\frac{1}{2}}\right)$ [50]. I_2 is the iteration number for **Algorithm 2** to converge. The convergence of **Algorithm 2** is guaranteed by the following proposition.

Proposition 4. Algorithm 2 is guaranteed to converge to a stationary point of problem (49).

Proof. Note that the objective function of (49) is bounded above by the objective function of (51). Each iteration of **Algorithm 2** gives a non-increasing objective function of (51). Thus, the proposed **Algorithm 2** can at least converge to a stationary point of (49). \square

E. The Overall Algorithm

The proposed algorithm for solving problem (23) is summarized in **Algorithm 3**, where $\mathcal{B}^{(j)} = \{\mathbf{w}_0^{(j)}, \mathbf{u}^{(j)}, \{\mathbf{u}_l^{(j)}\}_{l=1}^L, \{r_l^{(j)}\}_{l=1}^L\}$ and $\mathcal{C}^{(j)} = \{\mathbf{V}_r^{(j)}, \mathbf{V}_t^{(j)}\}$. The computational complexity of **Algorithm 3** is given by $\mathcal{O}(I_3(I_1(2(L+1)N_r^3 + (L+1)^{0.5}((L+1)N_t^2 + N_t^3)) + I_2 \max\{L+2, N\}^4 N^{\frac{1}{2}}))$, where I_3 is the iteration number for **Algorithm 3** to converge. Thanks to the generality of the STAR-RIS, the sum computation rate maximization

problem for traditional RIS aided ISCC systems can also be solved with the proposed algorithms, resulting in comparable computation complexity.

Proposition 5. Algorithm 3 is guaranteed to converge to a stationary point of problem (23).

Proof. At the $(j-1)$ -th iteration of the **Algorithm 3**, the step 4 gives objective function $R(\mathcal{B}^{(j)}, \mathcal{C}^{(j)})$. Based on **Proposition 3**, updating \mathcal{B} with fixed \mathcal{C} can at least give a non-decreasing objective function. It follows that $R(\mathcal{B}^{(j)}, \mathcal{C}^{(j)}) \leq R(\mathcal{B}^{(j+1)}, \mathcal{C}^{(j)})$.

At the j -th iteration of the **Algorithm 3**, the step 2 gives objective function $R(\mathcal{B}^{(j+1)}, \mathcal{C}^{(j)})$ and the step 4 gives objective function $R(\mathcal{B}^{(j+1)}, \mathcal{C}^{(j+1)})$. It follows that $R(\mathcal{B}^{(j+1)}, \mathcal{C}^{(j)}) = R(\mathcal{B}^{(j+1)}, \mathcal{C}^{(j+1)})$ since the objective function is regardless of STAR-RIS coefficients.

Then it follows that the sum computation rate is non-decreasing over every iteration of Algorithm 3, i.e.,

$$R(\mathcal{B}^{(j)}, \mathcal{C}^{(j)}) \leq R(\mathcal{B}^{(j+1)}, \mathcal{C}^{(j+1)}). \quad (52)$$

Recall that the sum computation rate of the ISCC system is bounded above due to the limited power budget at the BS. The proposed algorithm can reach at least a stationary point of problem (23). \square

The proposed algorithm is carried out at the BS (equipped with the edge server), and the required information exchanges between the BS, RIS, and decision robots in the proposed ISCC system include¹: (1) The BS sends the coefficient configuration to the STAR-RIS via the dedicated controller connecting the BS and RIS. (2) The BS feeds back the allocated offloading computation rate to each decision robot via downlink transmission links. (3) The decision robots offload their computation tasks to the edge server at the BS through uplink transmission links. (4) The BS returns the computation results to the decision robots via downlink transmission links.

IV. SIMULATION RESULTS

In this section, the simulation setup of the proposed ISCC IoRT system is introduced. Then, simulation results are provided to verify the effectiveness of the proposed algorithm for solving the sum computation rate maximization problem.

A. Simulation Setup

Fig. 3 depicts the simulation setup for the considered STAR-RIS aided ISCC IoRT system, where the BS is placed at the original point of the coordinate system and the STAR-RIS is placed at $(0, 20)$ (m). DRs are spread around the STAR-RIS and fall on the circles centered at the STAR-RIS with a radius of 5 m. The BS is assumed to be equipped with $N_t = 8$ transmit antennas and $N_r = 8$ receive antennas. The number of STAR-RIS elements is set as $N = 40$. The number of DRs L is set as an even number and all DRs are equally divided into the transmission and reflection sides of the STAR-RIS.

¹This work focuses on the uplink scenario, though the information exchanges between the BS and decision robots involve downlink transmission.

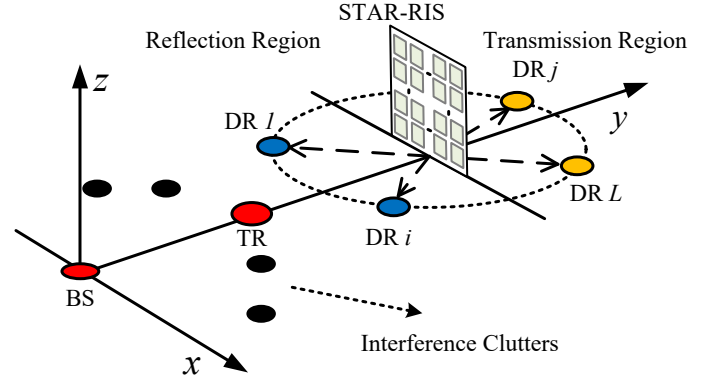


Fig. 3: Simulation setup for the STAR-RIS aided ISCC IoRT system.

The TR is set at $(0, 10)$ (m), while $M = 4$ interfere clusters fall on the circles centered at the original point with a radius of 10 m. The angles of interfere clusters are $\{\theta_1, \theta_2, \theta_3, \theta_4\} = \{-\frac{\pi}{3}, -\frac{\pi}{6}, \frac{\pi}{6}, \frac{\pi}{3}\}$.

The STAR-RIS can be deployed at a favorable position where the LoS channels can be established between both the BS and the STAR-RIS as well as the STAR-RIS and DRs [51]. Thus, the channels between the BS and the STAR-RIS as well as the channels between the STAR-RIS and DRs can be modeled with Rician fading, which can be expressed as follows:

$$\mathbf{h} = \sqrt{\beta} \left(\sqrt{\frac{\epsilon}{\epsilon + 1}} \mathbf{h}_{\text{LoS}} + \sqrt{\frac{1}{\epsilon + 1}} \mathbf{h}_{\text{NLoS}} \right), \quad (53)$$

where \mathbf{h}_{LoS} is the LoS channel component and the \mathbf{h}_{NLoS} is the NLoS channel component. ϵ is the Rician factor. $\beta = Dd^{-\alpha}$ represents the path loss coefficient, where $D = -30$ dB is the path loss at the reference distance 1 m. d is the transmission distance and α is the path loss exponent. When it comes to channels between the BS and the TR or interfere clusters, the Rician channel model is similar to (53) with different path loss coefficient β_s which can be expressed as $\beta_s = D(2d)^{-\alpha}$.

The penalty coefficients adopted in problem (49) is $\rho_r = \rho_t = 10^3$ [49]. The communication bandwidth for uplink offloading is set as $B = 20$ MHz. The power coefficient of the edge server is set as $\kappa = 10^{-26}$ [52]. The computation cycles required to process one bit of data at the edge server are set as $\phi = 3 \times 10^3$ cycle/bit. The noise power at the BS is -90 dBm. The transmit power of DRs is $P_u = 10$ dBm. The sensing threshold is $\Gamma_{\text{rad}} = 30$ dB. The power budget at the BS is $P_b = 30$ dBm. The Rician factor is set as $\epsilon = 3$ dB and the path loss factor is set as $\alpha = 2.2$.

B. Baseline Schemes

To verify the effectiveness and benefits of the proposed STAR-RIS aided ISCC IoRT system, we consider the following baseline schemes.

- 1) **Conventional RIS Scheme:** In this baseline scheme, we adopt two conventional RISs (one reflection RIS and one transmission RIS) deployed adjacent to each other to realize full space coverage. To provide a fair comparison, each RIS contains $N/2$ elements. This benchmark can be achieved with a STAR-RIS by setting $\rho_n^t = 1, \forall n \leq$

$N/2$, and $\rho_n^r = 1, \forall n > N/2$. The optimization problem that results from this configuration for RIS coefficients optimization can be given by

$$\text{Find } \mathbf{V}_i, \forall i \in \{t, r\} \quad (54a)$$

$$\text{s.t. } (46), (47c), (47d), \quad (54b)$$

$$\text{diag}(\mathbf{V}_t) = \text{Bdiag} \left\{ \mathbf{I}_{\frac{N}{2}}, \mathbf{0}_{\frac{N}{2}} \right\}, \quad (54c)$$

$$\text{diag}(\mathbf{V}_r) = \text{Bdiag} \left\{ \mathbf{0}_{\frac{N}{2}}, \mathbf{I}_{\frac{N}{2}} \right\}. \quad (54d)$$

This problem can be solved by Algorithm 2 with appropriate modification.

- 2) **Equal Splitting STAR-RIS Scheme:** In this baseline scheme, all STAR-RIS elements equally split the signal energy into the transmission and reflection sides. This benchmark can be achieved with a STAR-RIS by setting $\rho_n^t = \rho_n^r = 1/2, \forall n$. The optimization problem that results from this configuration for STAR-RIS coefficients optimization can be given by

$$\text{Find } \mathbf{V}_i, \forall i \in \{t, r\} \quad (55a)$$

$$\text{s.t. } (46), (47c), (47d), \quad (55b)$$

$$\text{diag}(\mathbf{V}_i) = \frac{1}{2} \mathbf{I}_N, \forall i \in \{t, r\}. \quad (55c)$$

This problem can be solved by Algorithm 2 with appropriate modification.

- 3) **Offloading Only Scheme:** In this baseline scheme, the BS only provides offloading computation service and does not carry out target sensing. Without the sensing to communication interference, the uplink communication SINR for DR l can be expressed as

$$\gamma_{u,l} = \frac{P_u |\mathbf{u}_l^H \mathbf{H}^H \Phi(l) \mathbf{h}_{u,l}|^2}{P_u \sum_{i \neq l} |\mathbf{u}_l^H \mathbf{H}^H \Phi(i) \mathbf{h}_{u,i}|^2 + \sigma_u^2 \|\mathbf{u}_l\|_2^2}. \quad (56)$$

The optimization problem that results from this configuration can be given by

$$\max_{\hat{\mathcal{A}}} R \quad (57a)$$

$$\text{s.t. } \sum_{l=1}^L \kappa(\phi r_l)^3 \leq P_b, \quad (57b)$$

$$(19c), (19e), (19e), (19e), \quad (57c)$$

where $\hat{\mathcal{A}} = \{\mathbf{u}, \{\mathbf{u}_l\}_{l=1}^L, \{r_l\}_{l=1}^L, \Phi_r, \Phi_t\}$. This problem can be solved by Algorithm 3 with appropriate modification.

In simulation figures, legends ‘‘Proposed STAR-RIS’’ represents the proposed STAR-RIS aided ISCC IoRT system. Legends ‘‘E-STAR-RIS’’ represents ISCC IoRT system with equal splitting STAR-RIS. Legends ‘‘C-RIS’’ represents the ISCC IoRT system with conventional RIS. Legends ‘‘Offloading Only’’ represents the IoRT system without the sensing requirement.

C. Simulation Results

The convergence of Algorithm 3 is analyzed in Fig. 4, illustrating the sum computation rate against the number of

AO iterations. The number of DRs and their transmit power are configured as $L = 4$ or 8 and $P_u = 10$ dBm or 15 dBm, respectively. It is clear that the algorithms converge after several iterations, with the sum computation rates of all instances consistently increasing with each iteration.

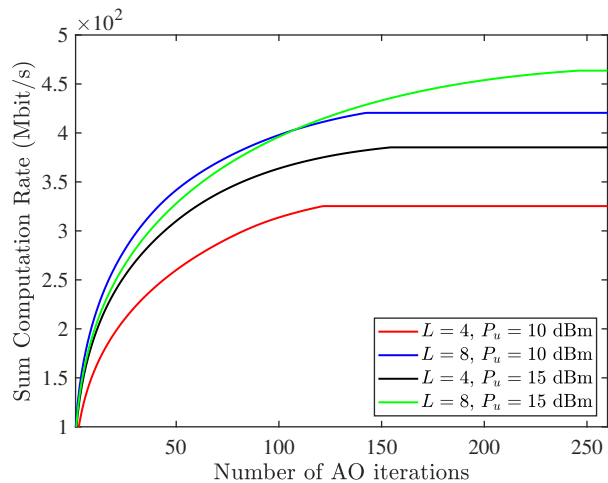


Fig. 4: The sum computation rate of DRs versus the number of AO iterations.

In Fig. 5, the computation rates achieved by different schemes are examined in relation to the power budget at the BS, with a fixed sensing threshold of $\Gamma_s = 30$ dB. It is observed that the sum computation rate of all schemes increases as the power budget at the BS increases. This is due to the increased available power at the BS, enabling the edge server to process more data when computation is constrained by limited power. However, as the power at the BS continues to increase, the sum computation rate reaches a plateau. This plateau is attributed to the capacity limit of uplink offloading. The proposed schemes demonstrate superior performance compared to all ISCC schemes. This is expected because STAR-RIS effectively manages inter-user interference for DRs’ uplink offloading and mitigates interference between sensing and communication, thereby enhancing computation performance within the ISCC system. The offloading-only scheme outperforms the ISCC schemes because all available power is allocated solely to the computation task at the BS.

Fig. 6 illustrates the sum computation rate plotted against the sensing threshold. The computation performance declines as the sensing threshold increases for all ISCC schemes. This trend is anticipated because allocating more power to the sensing function as the threshold increases constrains the available power for computation at the BS, reflecting the inherent offloading-sensing trade-off.

Fig. 7 depicts the total computation rate of DRs versus the number of RIS elements, where the power budget at the BS is set at 24 dBm and 30 dBm, respectively. It has been observed that as the number of RIS elements increases, the total computation rate also increases. Furthermore, an increase in the number of RIS elements leads to a larger performance difference between STAR-RIS and conventional RIS. This phenomenon occurs because more RIS elements provide ad-

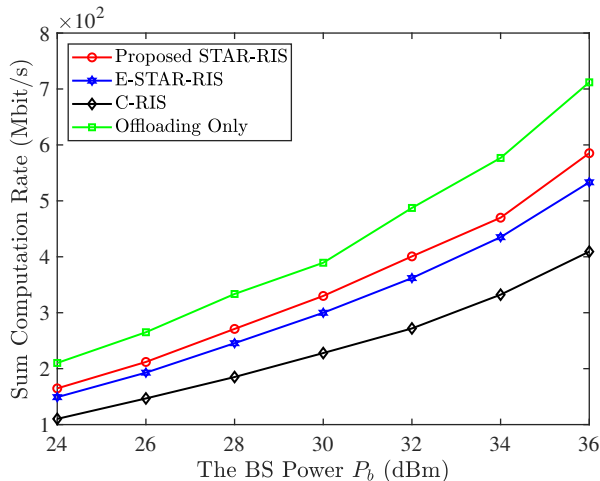


Fig. 5: The sum computation rate of DRs versus the power budget of the BS.

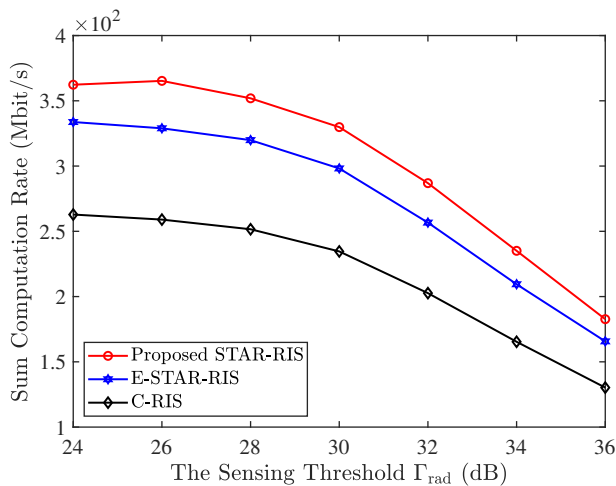


Fig. 6: The sum computation rate of DRs versus the sensing threshold. Additional opportunities to design more effective configuration strategies for STAR-RIS, thereby achieving greater performance benefits. The increase in computation rate brought by the addition of STAR-RIS elements is limited by the available power at the BS. When maintaining the minimum sensing SINR for the TR and performing computation at the edge server exhausts the BS's power budget, the computation rate at the BS reaches a plateau. This occurs because the BS lacks the capacity to provide additional computing resources, even though the increasing number of STAR-RIS elements can further enhance the offloading capacity between the BS and DRs.

In conclusion, when the computation rate at the BS is limited by the channel quality between the BS and DRs, increasing the number of STAR-RIS elements can effectively improve the computation rate. However, when the computation rate is limited by the power budget at the BS, further increasing the number of STAR-RIS elements does not provide additional benefits.

In Fig. 8, the sensing beampattern achieved by the proposed scheme with Algorithm 3. The normalized sensing beampat-

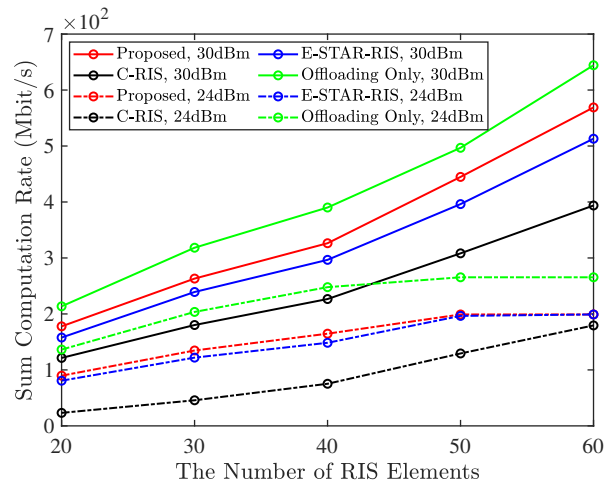


Fig. 7: The sum computation rate of DRs versus the number of RIS elements.

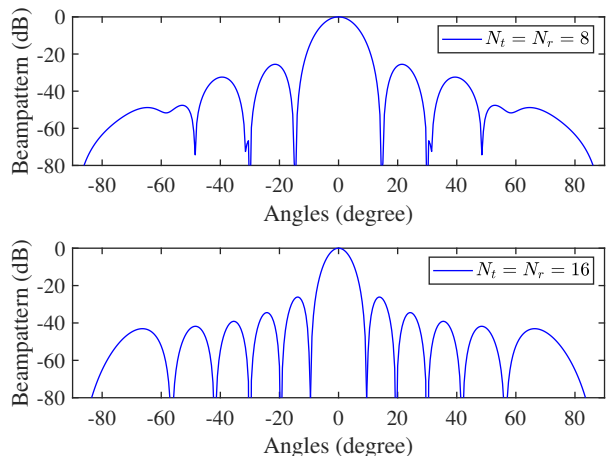


Fig. 8: The sensing beampattern achieved by Algorithm 3.

tern at angle θ is defined as

$$G(\theta) = \frac{|\mathbf{u}^H \mathbf{a}_r(\theta) \mathbf{a}_t(\theta)^H \mathbf{w}|^2}{\max_{\hat{\theta}} |\mathbf{u}^H \mathbf{a}_r(\hat{\theta}) \mathbf{a}_t(\hat{\theta})^H \mathbf{w}|^2}. \quad (58)$$

The main beam of the sensing beam pattern is focused on the TR, with several nulls deliberately positioned towards the interferers. This demonstrates the effectiveness of the proposed beamforming design for TR sensing in the presence of interfering clusters. Moreover, the 16-antenna system is capable of forming deeper nulls at the angles of the interferers.

V. CONCLUSION

This work proposed a STAR-RIS-aided ISCC IoRT framework, where the BS simultaneously senses the TR and computes data for DRs. To address the sum computation rate optimization problem, an AO algorithm was developed for beamforming design at the BS and coefficient optimization at the STAR-RIS. Simulation results were presented to demonstrate the convergence of the proposed algorithm. Additionally, the advantage of adopting STAR-RIS in the ISCC IoRT system was verified. This work confirms the effectiveness of utilizing

STAR-RIS to support communication and computation functions in ISCC IoRT systems. The potential of involving STAR-RIS not only in communication and computation but also in the sensing function can be an intriguing future research topic. Furthermore, given that the FD BS is adopted in the proposed ISCC systems, research on ISCC systems with simultaneous uplink offloading and downlink communication can be a promising direction for future exploration.

REFERENCES

- [1] M. R. Palattella, M. Dohler, A. Grieco, G. Rizzo, J. Torsner, T. Engel, and L. Ladid, "Internet of things in the 5G era: Enablers, architecture, and business models," *IEEE J. Sel. Areas Commun.*, vol. 34, no. 3, pp. 510–527, 2016.
- [2] U. M. Malik, M. A. Javed, S. Zeadally, and S. ul Islam, "Energy-efficient fog computing for 6G-enabled massive IoT: Recent trends and future opportunities," *IEEE Internet Things J.*, vol. 9, no. 16, pp. 14 572–14 594, 2021.
- [3] P. Simoens, M. Dragone, and A. Saffiotti, "The Internet of Robotic Things: A review of concept, added value and applications," *Int. J. Adv.*, vol. 15, no. 1, 2018.
- [4] P. P. Ray, "Internet of robotic things: concept, technologies, and challenges," *IEEE access*, vol. 4, pp. 9489–9500, 2016.
- [5] N. H. Motlagh, M. Bagaa, and T. Taleb, "UAV-based IoT platform: A crowd surveillance use case," *IEEE Commun. Mag.*, vol. 55, no. 2, pp. 128–134, 2017.
- [6] Y. Cui, F. Liu, X. Jing, and J. Mu, "Integrating sensing and communications for ubiquitous IoT: Applications, trends, and challenges," *IEEE Netw.*, vol. 35, no. 5, pp. 158–167, 2021.
- [7] Z. Chen, T. Zheng, C. Hu, H. Cao, Y. Yang, H. Jiang, and J. Luo, "ISACoT: Integrating sensing with data traffic for ubiquitous IoT devices," *IEEE Commun. Mag.*, vol. 61, no. 5, pp. 98–104, 2023.
- [8] S. Tayeb, S. Latifi, and Y. Kim, "A survey on IoT communication and computation frameworks: An industrial perspective," in *Proc. IEEE 7th Annu. Comput. Commun. Workshop Conf. (CCWC)*, 2017, pp. 1–6.
- [9] L. Xing, "Reliability in internet of things: Current status and future perspectives," *IEEE Internet Things J.*, vol. 7, no. 8, pp. 6704–6721, 2020.
- [10] X. Mu, Y. Liu, L. Guo, J. Lin, and R. Schober, "Intelligent reflecting surface enhanced indoor robot path planning: A radio map-based approach," *IEEE Trans. Wireless Commun.*, vol. 20, no. 7, pp. 4732–4747, 2021.
- [11] R. Zhong, X. Liu, Y. Liu, Y. Chen, and X. Wang, "Path design and resource management for NOMA enhanced indoor intelligent robots," *IEEE Trans. Wireless Commun.*, vol. 21, no. 10, pp. 8007–8021, 2022.
- [12] C. H. Everett, "Survey of collision avoidance and ranging sensors for mobile robots," *Rob. Auton. Syst.*, vol. 5, no. 1, pp. 5–67, 1989.
- [13] X. Shao, C. You, W. Ma, X. Chen, and R. Zhang, "Target sensing with intelligent reflecting surface: Architecture and performance," *IEEE J. Sel. Areas Commun.*, vol. 40, no. 7, pp. 2070–2084, 2022.
- [14] F. Spinelli and V. Mancuso, "Toward enabled industrial verticals in 5G: A survey on MEC-based approaches to provisioning and flexibility," *IEEE Commun. Surv. Tutor.*, vol. 23, no. 1, pp. 596–630, 2021.
- [15] Y. Mao, C. You, J. Zhang, K. Huang, and K. B. Letaief, "A survey on mobile edge computing: The communication perspective," *IEEE Commun. Surv. Tutor.*, vol. 19, no. 4, pp. 2322–2358, 2017.
- [16] D. Sabella, A. Vaillant, P. Kuure, U. Rauschenbach, and F. Giust, "Mobile-edge computing architecture: The role of MEC in the internet of things," *IEEE Consum. Electron. Mag.*, vol. 5, no. 4, pp. 84–91, 2016.
- [17] X. Qin, Z. Song, T. Hou, W. Yu, J. Wang, and X. Sun, "Joint resource allocation and configuration design for STAR-RIS-enhanced wireless-powered MEC," *IEEE Trans. Commun.*, vol. 71, no. 4, pp. 2381–2395, 2023.
- [18] M. Di Renzo, A. Zappone, M. Debbah, M.-S. Alouini, C. Yuen, J. de Rosny, and S. Tretjakov, "Smart radio environments empowered by reconfigurable intelligent surfaces: How it works, state of research, and the road ahead," *IEEE J. Sel. Areas Commun.*, vol. 38, no. 11, pp. 2450–2525, 2020.
- [19] C. Pan, G. Zhou, K. Zhi, S. Hong, T. Wu, Y. Pan, H. Ren, M. D. Renzo, A. Lee Swindlehurst, R. Zhang, and A. Y. Zhang, "An overview of signal processing techniques for RIS/IRS-aided wireless systems," *IEEE J. Sel. Top. Signal Process.*, vol. 16, no. 5, pp. 883–917, 2022.
- [20] X. Mu, J. Xu, Z. Wang, and N. Al-Dhahir, "Simultaneously transmitting and reflecting surfaces for ubiquitous next generation multiple access in 6G and beyond," *Proc. of the IEEE*, pp. 1–26, 2024, doi: 10.1109/JPROC.2024.3405351.
- [21] N. Huang, C. Dou, Y. Wu, L. Qian, and R. Lu, "Energy-efficient integrated sensing and communication: A multi-access edge computing design," *IEEE Wireless Commun. Lett.*, vol. 12, no. 12, pp. 2053–2057, 2023.
- [22] N. Huang, C. Dou, Y. Wu, L. Qian, B. Lin, and H. Zhou, "Unmanned aerial vehicle aided integrated sensing and computation with mobile edge computing," *IEEE Internet Things J.*, vol. 10, no. 19, pp. 16 830–16 844, 2023.
- [23] Y. Xu, T. Zhang, Y. Liu, and D. Yang, "UAV-enabled integrated sensing, computing, and communication: A fundamental trade-off," *IEEE Wireless Commun. Lett.*, vol. 12, no. 5, pp. 843–847, 2023.
- [24] C. Ding, J.-B. Wang, H. Zhang, M. Lin, and G. Y. Li, "Joint MIMO precoding and computation resource allocation for dual-function radar and communication systems with mobile edge computing," *IEEE J. Sel. Areas Commun.*, vol. 40, no. 7, pp. 2085–2102, 2022.
- [25] L. Zhao, D. Wu, L. Zhou, and Y. Qian, "Radio resource allocation for integrated sensing, communication, and computation networks," *IEEE Trans. Wireless Commun.*, vol. 21, no. 10, pp. 8675–8687, 2022.
- [26] N. Huang, C. Dou, Y. Wu, L. Qian, B. Lin, H. Zhou, and X. Shen, "Mobile edge computing aided integrated sensing and communication with short-packet transmissions," *IEEE Trans. Wireless Commun.*, vol. 23, no. 7, pp. 7759–7774, 2024.
- [27] K. Cheng, X. Fang, and X. Wang, "Optimized resource allocation and time partitioning for integrated communication, sensing, and edge computing network," *Comput. Commun.*, vol. 194, pp. 240–249, 2022.
- [28] Y. He, G. Yu, Y. Cai, and H. Luo, "Integrated sensing, computation, and communication: System framework and performance optimization," *IEEE Trans. Wireless Commun.*, vol. 23, no. 2, pp. 1114–1128, 2024.
- [29] N. Huang, T. Wang, Y. Wu, Q. Wu, and T. Q. Quek, "Integrated sensing and communication assisted mobile edge computing: An energy-efficient design via intelligent reflecting surface," *IEEE Wireless Commun. Lett.*, vol. 11, no. 10, pp. 2085–2089, 2022.
- [30] S. Xu, Y. Du, J. Zhang, J. Liu, J. Wang, and J. Zhang, "Intelligent reflecting surface enabled integrated sensing, communication and computation," *IEEE Trans. Wireless Commun.*, vol. 23, no. 3, pp. 2212–2225, 2024.
- [31] Y. Liu, X. Mu, J. Xu, R. Schober, Y. Hao, H. V. Poor, and L. Hanzo, "STAR: Simultaneous transmission and reflection for 360° coverage by intelligent surfaces," *IEEE Wireless Commun.*, vol. 28, no. 6, pp. 102–109, 2021.
- [32] J. Lei, T. Zhang, X. Mu, and Y. Liu, "NOMA for STAR-RIS assisted UAV networks," *IEEE Trans. Commun.*, vol. 72, no. 3, pp. 1732–1745, 2024.
- [33] C. Wu, Y. Liu, X. Mu, X. Gu, and O. A. Dobre, "Coverage characterization of STAR-RIS networks: NOMA and OMA," *IEEE Communications Letters*, vol. 25, no. 9, pp. 3036–3040, 2021.
- [34] B. P. Day, A. R. Margetts, D. W. Bliss, and P. Schniter, "Full-duplex MIMO relaying: Achievable rates under limited dynamic range," *IEEE J. Sel. Areas Commun.*, vol. 30, no. 8, pp. 1541–1553, 2012.
- [35] A. Sabharwal, P. Schniter, D. Guo, D. W. Bliss, S. Rangarajan, and R. Wichman, "In-band full-duplex wireless: Challenges and opportunities," *IEEE J. Sel. Areas Commun.*, vol. 32, no. 9, pp. 1637–1652, 2014.
- [36] K. E. Kolodziej, B. T. Perry, and J. S. Herd, "In-band full-duplex technology: Techniques and systems survey," *IEEE Trans. Microw. Theory Tech.*, vol. 67, no. 7, pp. 3025–3041, 2019.
- [37] F. Liu, Y. Cui, C. Masouros, J. Xu, T. X. Han, Y. C. Eldar, and S. Buzzi, "Integrated sensing and communications: Toward dual-functional wireless networks for 6G and beyond," *IEEE J. Sel. Areas Commun.*, vol. 40, no. 6, pp. 1728–1767, 2022.
- [38] W. L. Stutzman and G. A. Thiele, *Antenna Theory and Design*. Hoboken, NJ, USA: Wiley, 2012.
- [39] R. Liu, M. Li, Y. Liu, Q. Wu, and Q. Liu, "Joint transmit waveform and passive beamforming design for RIS-aided DFRC systems," *IEEE J. Sel. Top. Signal Process.*, vol. 16, no. 5, pp. 995–1010, 2022.
- [40] N. I. Miridakis and D. D. Vergados, "A survey on the successive interference cancellation performance for single-antenna and multiple-antenna OFDM systems," *IEEE Commun. Surv. Tutor.*, vol. 15, no. 1, pp. 312–335, 2013.
- [41] G. Cui, H. Li, and M. Rangaswamy, "MIMO radar waveform design with constant modulus and similarity constraints," *IEEE Trans. Signal Process.*, vol. 62, no. 2, pp. 343–353, 2013.
- [42] D. Tse and P. Viswanath, *Fundamentals of Wireless Communication*. Cambridge, U.K.: Cambridge Univ. Press, 2005.

- [43] Q. Shi, M. Razaviyayn, Z.-Q. Luo, and C. He, "An iteratively weighted MMSE approach to distributed sum-utility maximization for a MIMO interfering broadcast channel," *IEEE Trans. Signal Process.*, vol. 59, no. 9, pp. 4331–4340, 2011.
- [44] M. Grant and S. Boyd, "CVX: Matlab software for disciplined convex programming, version 2.1," [Online]. Available: <http://cvxr.com/cvx>, 2014.
- [45] R. A. Horn and C. R. Johnson, *Matrix Analysis*. Cambridge, U.K.: Cambridge Univ. Press, 2012.
- [46] Y. Nesterov and A. Nemirovskii, *Interior-point Polynomial Algorithms in Convex Programming*. Philadelphia, PA, USA: SIAM, 1994.
- [47] A. Ben-Tal and M. Zibulevsky, "Penalty/barrier multiplier methods for convex programming problems," *SIAM J. Optim.*, vol. 7, no. 2, pp. 347–366, 1997. [Online]. Available: <https://doi.org/10.1137/S1052623493259215>
- [48] X. Mu, Y. Liu, L. Guo, J. Lin, and R. Schober, "Simultaneously transmitting and reflecting (STAR) RIS aided wireless communications," *IEEE Trans. Wireless Commun.*, vol. 21, no. 5, pp. 3083–3098, 2021.
- [49] D. Xu, X. Yu, Y. Sun, D. W. K. Ng, and R. Schober, "Resource allocation for IRS-assisted full-duplex cognitive radio systems," *IEEE Trans. Commun.*, vol. 68, no. 12, pp. 7376–7394, 2020.
- [50] Z.-Q. Luo, W.-K. Ma, A. M.-C. So, Y. Ye, and S. Zhang, "Semidefinite relaxation of quadratic optimization problems," *IEEE Signal Process. Mag.*, vol. 27, no. 3, pp. 20–34, 2010.
- [51] M. Hua and Q. Wu, "Throughput maximization for IRS-aided MIMO FD-WPCN with non-linear EH model," *IEEE J. Sel. Top. Signal Process.*, vol. 16, no. 5, pp. 918–932, 2022.
- [52] Z. Wang, X. Mu, Y. Liu, X. Xu, and P. Zhang, "NOMA-aided joint communication, sensing, and multi-tier computing systems," vol. 41, no. 3, pp. 574–588, 2023.



Xidong Mu (Member, IEEE, <https://xidongmu.github.io/>) received the Ph.D. degree in Information and Communication Engineering from the Beijing University of Posts and Telecommunications, Beijing, China, in 2022.

He was with the School of Electronic Engineering and Computer Science, Queen Mary University of London, from 2022 to 2024, where he was a Postdoctoral Researcher. He has been a lecturer (an assistant professor) with the Centre for Wireless Innovation (CWI), Queen's University Belfast, U.K. since August 2024. His research interests include non-orthogonal multiple access (NOMA), IRSs/RISs aided communications, integrated sensing and communications, semantic communications, and optimization theory. He received the IEEE ComSoc Outstanding Young Researcher Award for EMEA region in 2023, the Exemplary Reviewer Certificate of the IEEE TRANSACTIONS ON COMMUNICATIONS in 2020 and 2022, and the IEEE COMMUNICATION LETTERS in 2021–2023. He is the recipient of the 2024 IEEE Communications Society Heinrich Hertz Award, the Best Paper Award in ISWCS 2022, the 2022 IEEE SPCC-TC Best Paper Award, and the Best Student Paper Award in IEEE VTC2022-Fall. He serves as the Public Engagement and Social Networks Coordinator of IEEE ComSoc SPCC Technical Committee, the secretary of the IEEE ComSoc Next Generation Multiple Access (NGMA) Emerging Technology Initiative and the Special Interest Group (SIG) in SPCC Technical Committee on Signal Processing Techniques for NGMA. He also serves as an Editor of IEEE TRANSACTIONS ON COMMUNICATIONS, a Guest Editor for IEEE TRANSACTIONS ON COGNITIVE COMMUNICATIONS AND NETWORKING Special Issue on "Machine Learning and Intelligent Signal Processing for Near-Field Technologies", IEEE INTERNET OF THINGS JOURNAL Special Issue on "Next Generation Multiple Access for Internet-of-Things", the NGMA workshop co-chairs of IEEE WCNC 2023, IEEE PIMRC 2023, and IEEE GLOBECOM 2023, and the "Mobile and Wireless Networks" symposium co-chair of IEEE GLOBECOM 2025.



Haochen Li (Graduate Student Member, IEEE) received the B.S. degree in communication engineering from Nanjing University of Science and Technology, Nanjing, China, in 2019. He is currently pursuing the Ph.D. degree with the National Mobile Communications Research Laboratory, Southeast University, Nanjing, China. He is also a Research Associate with the School of Electronic Engineering and Computer Science, Queen Mary University of London, since September 2022. His current research interests include massive MIMO

communication, reconfigurable intelligent surface, and integrated sensing and communications.



Yuanwei Liu (Fellow, IEEE, <http://www.eecs.qmul.ac.uk/~yuanwei>) has been a (tenured) full Professor in Department of Electrical and Electronic Engineering (EEE) at The University of Hong Kong (HKU) since September, 2024. Prior to that, he was a Senior Lecturer (Associate Professor) (2021-2024) and a Lecturer (Assistant Professor) (2017- 2021) at Queen Mary University of London (QMUL), London, U.K, and a Postdoctoral Research Fellow (2016-2017) at King's College London (KCL), London, U.K. He received the Ph.D. degree from QMUL

in 2016. His research interests include non-orthogonal multiple access, reconfigurable intelligent surface, near field communications, integrated sensing and communications, and machine learning.

Yuanwei Liu is a Fellow of the IEEE, a Fellow of AAIA, a Web of Science Highly Cited Researcher, an IEEE Communication Society Distinguished Lecturer, an IEEE Vehicular Technology Society Distinguished Lecturer, the rapporteur of ETSI Industry Specification Group on Reconfigurable Intelligent Surfaces (RIS): Modelling, Optimisation, and Operation”, and the UK representative for the URSI Commission C on “Radio communication Systems and Signal Processing”. He was listed as one of 35 Innovators Under 35 China in 2022 by MIT Technology Review. He received IEEE ComSoc Outstanding Young Researcher Award for EMEA in 2020. He received the 2020 IEEE Signal Processing and Computing for Communications (SPCC) Technical Committee Early Achievement Award, IEEE Communication Theory Technical Committee (CTTC) 2021 Early Achievement Award. He received IEEE ComSoc Outstanding Nominee for Best Young Professionals Award in 2021. He is the co-recipient of the 2024 IEEE Communications Society Heinrich Hertz Award, the Best Student Paper Award in IEEE VTC2022-Fall, the Best Paper Award in ISWCS 2022, the 2022 IEEE SPCC-TC Best Paper Award, the 2023 IEEE ICCT Best Paper Award, and the 2023 IEEE ISAP Best Emerging Technologies Paper Award. He serves as the Co-Editor-in-Chief of IEEE ComSoc TC Newsletter, an Area Editor of IEEE Communications Letters, an Editor of IEEE Communications Surveys & Tutorials, IEEE Transactions on Wireless Communications, IEEE Transactions on Vehicular Technology, IEEE Transactions on Network Science and Engineering, IEEE Transactions on Cognitive Communications and Networking, and IEEE Transactions on Communications (2018-2023). He serves as the (leading) Guest Editor for Proceedings of the IEEE on Next Generation Multiple Access, IEEE JSAC on Next Generation Multiple Access, IEEE JSTSP on Intelligent Signal Processing and Learning for Next Generation Multiple Access, and IEEE Network on Next Generation Multiple Access for 6G. He serves as the Publicity Co-Chair for IEEE VTC 2019-Fall, the Panel Co-Chair for IEEE WCNC 2024, Symposium Co-Chair for several flagship conferences such as IEEE GLOBECOM, ICC and VTC. He serves the academic Chair for the Next Generation Multiple Access Emerging Technology Initiative, vice chair of SPCC and Technical Committee on Cognitive Networks (TCCN).



Pan Zhiwen (Member, IEEE) is currently a Professor with the National Mobile Communications Research Laboratory, Southeast University, Nanjing, China. During 2000–2001, he was involved in the research and standardization of 3G, and since 2002, he has been involved in the investigations on key technologies for IMT-A, 5G and 6G. He has authored or coauthored more than 50 papers recently, and holds more than 70 patents. His research interests include self-organizing networks, wireless networking, and radio transmission technology for

wireless communications.



Yue Chen (Senior Member, IEEE) received the B.Eng. and M.Eng. degrees from the Beijing University of Posts and Telecommunications (BUPT), Beijing, China, in 1997 and 2000, respectively, and the Ph.D. degree from QMUL, London, U.K., in 2003.

She is currently a Professor of Telecommunications Engineering at the School of Electronic Engineering and Computer Science, Queen Mary University of London (QMUL), U.K. Her current research interests include wireless communication

networks, mobile edge computing, smart energy systems, and the Internet of Things.